PHYSICAL REVIEW MATERIALS **8**, 045601 (2024)

Bidisperse ring polymers: Topological glass to stacking

Projesh Kumar Roy,[*] Pinaki Chaudhuri,[†] and Satyavani Vemparala[‡]
The Institute of Mathematical Sciences, C.I.T. Campus, Taramani, Chennai 600113, India
and Homi Bhabha National Institute, Training School Complex, Anushakti Nagar, Mumbai 400094, Maharashtra, India

(Received 18 May 2023; accepted 22 March 2024; published 5 April 2024)

Via large-scale molecular dynamics simulations, we observe the melting of a topological glass of stiff ring polymers by incorporating flexible ring polymers, along an isobaric path. As more flexible ring polymers are introduced, stacked glassy structures emerge in the stiffer ring polymers with reduced orthogonal threading. This eventually evolves to a stacked columnar structure at an increased fraction of flexible ring polymers. Depletion interactions between the stiff and flexible rings drive the stacking, contingent on the disparity in flexibility in the ring polymer mixture.

DOI: 10.1103/PhysRevMaterials.8.045601

I. INTRODUCTION

The emergence of self-organized ordered structures in soft materials is well established now [1–4]. Two primary routes that lead to such ordering are effective hardcore [5–7] and depletion interactions [8–12]. For example, various studies on mixtures of nondeformable hard sphere colloidal systems have shown that such systems exhibit rich phases including crystalline and amorphous states as a function of the ratio of hard sphere sizes [13–19]. However, the exploration of parameter space for mixtures of hardcore objects is limited. Introducing deformability could substantially enhance the availability of viable structures and lead to the emergence of interesting nonequilibrium or kinetically trapped phases.

Ring polymers with easily controllable backbone stiffness have emerged as excellent model systems for understanding the emergence of phase behavior in soft and deformable colloidal systems with tuneable interactions [20–23]. Recent studies have demonstrated the emergence of glasslike states for dense ring polymer systems, which are inaccessible to their linear counterparts [24–28]. Known as topological glasses, these glassy states are deemed to occur via the interpenetration of rings (termed as threading) due to the existence of closed-loop topological constraints [29–36]. For stiff enough rings, such glassy states consist of clustered structures, and are therefore labeled as cluster glasses [37–41]. Moreover, we recently [42] showed that by carefully tuning the ring polymer stiffness, glassy states become easily accessible even at lower densities, without any artificial interventions [24–26].

In this study, we investigate how the mixing of rings with varying stiffness affects the stability of such topological glassy states. Our motivation stems from recent studies that explore such mixing effects in other deformable soft objects, such as linear polymers [43–46] and mixtures of soft and hard colloids [47,48]. These studies have demonstrated the significance of entropic effects in determining the emergent phase behavior [49]. Recent findings [50,51] also suggest that ring polymers could be stronger depleting agents than their linear polymers, indicating the potential for exotic self-assembly of topologically constrained deformable objects via depletion interactions.

Using extensive molecular dynamics (MD) simulations, we report the emergence of ordered aggregates, in the form of columnar stacked structures, in a binary mixture of ring polymers with different stiffness parameters, via a demixing process. We investigate the conformational landscape of the formation of such soft ordered aggregates of stiffer rings by exploring the binary mixture ratio of different ring polymer stiffness.

After the initial introductory discussion presented in Sec. I, we provide the details of the studied model and the various measured observables in Sec. II. In Sec. III, we discuss our findings, and Sec. IV has the conclusions.

II. MODEL AND METHODS

A. The model

We consider a mixture of ring polymers that are identical in size (i.e., they have the same number of monomers) but differ in stiffness parameters, K_θ^A (flexible A type) and K_θ^B (stiffer B type). In this study, we primarily focus on a mixture of B-type rings with stiffness $K_\theta^B = 20.0$ and A-type rings with stiffness $K_\theta^A = 1$. We vary the composition (A:B) of the mixture and explore the phase behavior at different thermodynamic state points for each composition. Additionally, we examine a few cases where $K_\theta^A = 5$ or 10 has been considered, which will be discussed in detail later.

Similar to our previous work [42], we employ the Kremer-Grest (KG) bead-spring model [52–54] to describe the interactions between monomers constituting the rings. The KG model comprises several components:

---

[*] projeshkr@imsc.res.in

[†] pinakic@imsc.res.in

[‡] vani@imsc.res.in

2475-9953/2024/8(4)/045601(8)

TABLE I. Force-field parameters: Monomers of A type belong to ring polymers with stiffness $K_\theta^A = 1.0$–10.0 and B type belongs to ring polymers with $K_\theta^B = 20.0$. The force-field parameters are represented in their usual symbols, see Ref. [42] for detailed descriptions.

Parameter	Value
$\sigma_{AA} = \sigma_{BB} = \sigma_{AB}$	$1.0\ \sigma$
$\epsilon_{AA} = \epsilon_{BB} = \epsilon_{AB}$	$1.0\ \mathrm{k_B}T$
$\kappa_{AA} = \kappa_{BB}$	$30.0\ \mathrm{k_B}T/\sigma^2$
$R_{0,AA} = R_{0,BB}$	$1.5\ \sigma$
K_θ^A	$1.0\ \mathrm{k_B}T$, $5.0\ \mathrm{k_B}T$, $10.0\ \mathrm{k_B}T$
K_θ^B	$20.0\ \mathrm{k_B}T$

(i) A Weeks-Chandler-Anderson (WCA) potential [55], representing the pairwise nonbonded interactions between any two monomers i, j separated by a distance r_{ij}:

$$U_{\rm WCA}(r_{ij}) = \begin{cases} 4\epsilon\left[\left(\frac{\sigma}{r_{ij}}\right)^{12} - \left(\frac{\sigma}{r_{ij}}\right)^{6} + \frac{1}{4}\right] & r_{ij} \leqslant 2^{1/6}\sigma \\ 0 & r_{ij} > 2^{1/6}\sigma. \end{cases}$$

(ii) A finitely extensible nonlinear elastic (FENE) potential [52] represents the bonded interactions between two consecutive monomers i, j in a polymer chain, separated by a distance d_{ij}:

$$U_{\rm FENE}(d_{ij}) = \begin{cases} -0.5\kappa R_0^2 \ln\left[1 - \left(\frac{d_{ij}}{R_0}\right)^2\right] & d_{ij} < R_0 \\ \infty & d_{ij} \geqslant R_0. \end{cases}$$

(iii) The Kratky-Porod angular potential [56,57] accounts for the stiffness of the rings by constraining the central angle θ between three consecutive monomers i, j, k in a polymer chain:

$$U_{\rm Angle}(\theta) = K_\theta[1 - cos(\theta - \pi)].$$

The force-field parameters for these interactions are detailed in Table I.

We have adopted the reduced unit formalism to express all variables in this paper. The unit of time is defined as $\tau = \sigma\sqrt{m/k_{\rm B}T}$, where m is the mass of the monomers and $k_{\rm B}T$ represents the thermal energy unit. We have assigned the mass of each monomer a value of 1.0. Accordingly, energies and length scales are expressed in terms of $k_{\rm B}T$ and σ, respectively. The equations of motion for the monomers that constitute the ring polymers are numerically integrated using the LAMMPS software package [58].

B. Simulation details

The system under investigation comprises 400 nonconcatenated ring polymers, each containing 100 monomers, resulting in a total of 4×10^4 particles. The system size was carefully selected to be large enough to mitigate self-interactions arising from periodic boundary conditions. Specifically, the box length in any direction at equilibrium, $L \approx 40\sigma$, exceeds the diameter of a B-type ring ($2\langle R_g\rangle \approx 29\sigma$) in all simulations [42], ensuring that $(L/2 - R_g) > 2^{1/6}\sigma$, where R_g denotes the radius of gyration. Furthermore, to investigate finite-size effects on structure formation, a larger system consisting of 1000 ring polymers, or 10^5 particles in total, was also examined.

Initial system configurations were generated at a very low density (4×10^{-5}) by randomly distributing the rings of the two species within the simulation box. The system's pressure was gradually increased to the target level in NPT simulations using a small timestep of 0.003, followed by MD simulations that continued until energy and density fluctuations stabilized (refer to Fig. S1 in the Supplemental Material [59]). From these initial runs, production runs spanning 10^8 steps were conducted for each system configuration, employing a timestep of 0.006τ. Throughout these simulations, the temperature and pressure were maintained at $T = 1.0$ and $P = 1.0$, respectively, using the overdamped Nosé-Hoover thermostat [60,61] and barostat [62], with a coupling timescale of $t_d = 1.0$.

III. RESULTS

The starting point of our study is a state point explored in our previous study [42], where a system of rings having a stiffness $K_\theta = 20.0$ showed glassy dynamics at ambient pressure of $P = 1.0$ and temperature $T = 1.0$. Such a glassy state has a topological nature, i.e., the glassiness primarily arises from the threading of the rings. A snapshot of such a structure is shown in Fig. 1(a), where the disorderedness of the assembly is evident (also see movie 1 in the SM [59]).

Our objective is to understand how the insertion of the more flexible A-type rings changes the structural and dynamical properties of the topological glass formed by the B-type stiffer rings, with changing composition of the A:B binary mixture at a fixed pressure and temperature. For the main part of our discussions, we focus on the mixture consisting of highly contrasting stiffness, viz. $K_\theta^A = 1.0$ and $K_\theta^B = 20.0$. At a pressure of $P = 1.0$, the stiffer single polymer adopts a nearly planar ring shape, while the more flexible polymer forms a compact globular structure [42]. Additionally, in the A-type=100% state, where only the highly flexible rings are present, the system is in a liquid state at this pressure [42]. Thus, we are probing what are the intermediate states in the A-B phase diagram, as we vary the composition along an isobaric path. Subsequently, we extend our discussion to encompass the influence of varying K_θ^A within the mixture on the manifested behaviors.

A. Probing phase behavior along isobaric path

In Figs. 1(a)–1(j), we show the emergent structures, sampled at long times, via the interplay of the rings having two different stiffness parameters. The striking finding is that the disordered structure formed by the stiffer B-type rings in the absence of A-type flexible rings evolves into a completely different structure with increasing fractions of the more flexible rings. Even at a small concentration of the A-type rings (e.g., 10%), the emergence of local stacking is visible, i.e., partial axial ordering of the stiffer rings is observed due to the intermixing of the two species (see movie 2 in SM [59]). As the concentration of A-type rings increases, these stacks become more pronounced. Eventually, at the dilute composition of the B-type rings, when the percentage of A-type rings exceeds 60% [see Figs. 1(h)–1(j)], intertwined stacks are formed, gradually reducing to a single stack at lowest

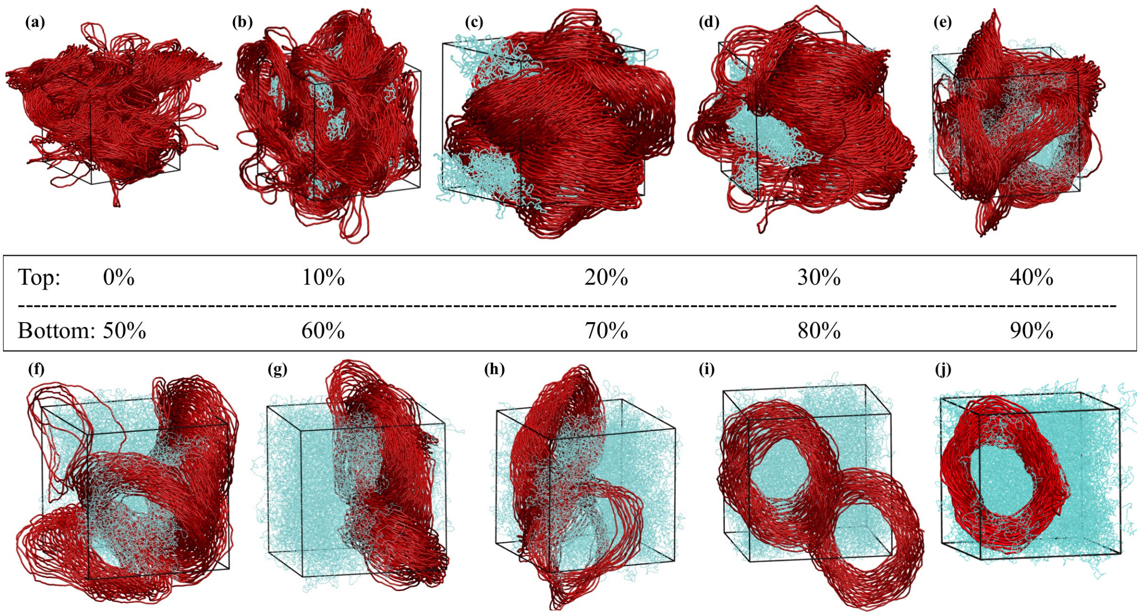

FIG. 1. (a)–(j) Snapshots of the binary mixture of ring polymers having stiffness $K_\theta^A = 1.0$ and $K_\theta^B = 20.0$ at ambient pressure $P = 1.0$ and temperature $T = 1.0$, labeled via concentration of A-type rings. Color code: Cyan=A-type, Red=B-type rings.

concentrations of B-type rings. Overall, the images in Fig. 1 clearly illustrate the melting of the topological glass formed by the stiffer rings as the more flexible rings are increasingly inserted. Subsequently, a demixing transition between the two species ultimately results in the formation of more ordered structures in the form of columnar stacks by the B-type stiffer rings.

B. Analysis of stacking

To quantify the observable stacking behavior of the B-type rings (see Fig. 1), we utilize the algorithm by Poier *et al.* [39,40], which enables the identification of neighboring rings that form stacks. The methodology unfolds as follows: First, for each ith ring, the eigenvectors ($\boldsymbol{d}_{\rm min,\,i}$) associated with the lowest eigenvalues are identified, assumed to be oriented almost perpendicularly to the ring's minimal plane. Subsequently, neighboring rings (j) are pinpointed whose center-of-mass vectors ($\boldsymbol{r}_{\rm COM,\,ij}$) align relatively parallel to the ith ring's minimal eigenvector; that is, $\theta_{ij} \leqslant 10^\circ$. The rings are further filtered to exclude distant ones by applying a stricter distance criterion: $|\boldsymbol{r}_{\rm COM,\,ij}|\| \leqslant 2.0$ and $|\boldsymbol{r}_{\rm COM,\,ij}|\perp \leqslant 2.0$. A connectivity matrix $M_{\rm st}$ of size $R \times R$ is then constructed, with its components $M_{\rm st}(i, j) = 1$ if the ith and jth rings stack against each other, and zero otherwise. Utilizing the connectivity matrix, stacks are identified by selecting sets of rings that are interconnected exclusively among themselves. To assess the impact of large stacks on the system's dynamics, any grouping with fewer than $C_{\rm min}$ rings is not considered a stack.

Through this analysis, we can also quantify the number of unstacked stiff rings and thereby compute the average fraction of unstacked rings ($f_{\rm us}$), which exhibits a marked decrease beyond a certain composition and limiting stack size [see Fig. 2(a)]. We use values of $C_{\rm min} = 5$, 10 to define a stack. The stacking analysis strongly suggests that the tendency to stack increases with the growing concentration of A-type rings. Signatures of unstacking are also evident through a decrease in the potential energy of the B-type rings; see Fig. S2 of the Supplemental Material (SM) [59]. Our observations are summarized in the form of a phase diagram in the space of average densities of A-type (ρ_A) and B-type (ρ_B) rings [see Fig. 2(b)], with the line marking the isobaric path that we have traversed in our study.

C. Analysis of threading

Next, we examine how the introduction of flexible rings influences the threading among the stiffer rings, which underpins the formation of the topological glass in the pure B-type system at $P = 1.0$. We calculated the net quantity of self-threading within the set of B-type rings in terms of an average threading parameter, $\langle \Delta_{\rm th} \rangle$. For details on the algorithm used to determine $\langle \Delta_{\rm th} \rangle$, see Ref. [42] and Sec. SIV of the Supplemental Material [59].

The net threading events between ring one and ring two can be quantified as an order parameter as

$$\Delta_{\rm th} = 1 - \left| \frac{2\sum_{i={\rm odd}} N^i_{\rm th}}{N_{\rm ring}} - 1 \right|, \tag{1}$$

where $N_{\rm ring}$ represents the total number of monomers in ring 1, $\Delta_{\rm th}$ denotes the degree of threading between ring 1 and ring 2, which have at least one crossing event between them, and $N^i_{\rm th}$ signifies the total number of monomers of ring 1 that have crossed the minimal surface of ring 2. The mean degree of threading, $\langle \Delta_{\rm th} \rangle$, is determined by averaging over all $\Delta_{\rm th}$ values with all other ring polymers for all the sampled trajectories. Up to five monomers are coarse grained to reduce computational costs. This coarse graining did not have any effect on the trend of $|\Delta_{\rm th}|$. By measuring the average threading parameter $\langle \Delta_{\rm th} \rangle$ among the stiff rings, we observe a decrease in threading at high dilutions [see Fig. 2(c)], accompanied

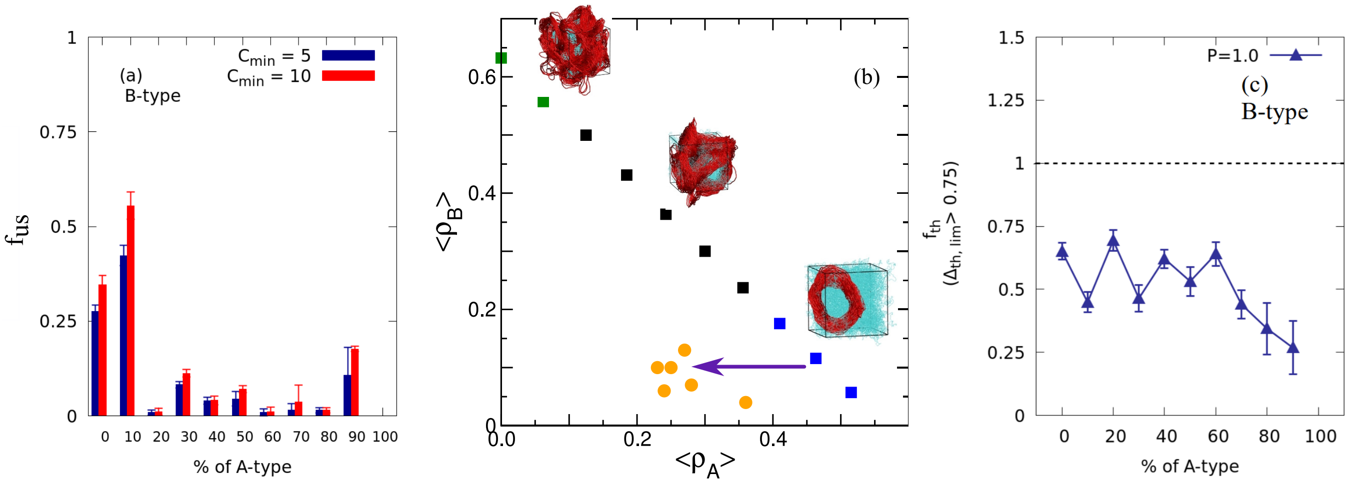

FIG. 2. (a) Variation of the average fraction of unstacked B-type rings, f_{us}, with different limiting stack sizes (C_{min}), as the concentration of A-type rings changes. (b) A phase diagram in the space of the obtained average densities of A-type and B-type rings, with squares marking the states visited during the isobaric examination at $P = 1$. Different structures obtained for the B-type rings are labeled with different colors, with adjoining images illustrating corresponding structures—namely glass, gel, and stacks. The orange circles mark the limit of stability of the stacks at smaller densities. (c) Variation of the fraction of highly threaded rings (f_{th}) with $\Delta_{\text{th,lim}} > 0.75$ of B-type rings (see text).

by corresponding ordering in the stack angle distribution. It is important to note that our threading detection algorithm neglects the peripheral threading of two flexible rings lying atop each other, achieved through coarse graining.

D. Probing stack stability via pressure cycles

A pertinent question to consider is whether the stacks of stiffer rings, observed at lower ρ_B values along the $P = 1$ isobaric path, represent stable and reproducible structures. To investigate this, we used the stacked states observed with a percentage of A-type rings exceeding 70% as initial conditions; we first decompressed these states to low pressure and then compressed them back to $P = 1$ at the same rate. This procedure was carried out for compositions of 90:10, 80:20, and 70:30. A single compression-decompression cycle consists of (i) reducing the pressure from $P = 1$ to $P = 0.01$ over a period of $t = 6 \times 10^5$, i.e., at a rate of $\dot{P} = 1.65 \times 10^{-6}$; (ii) then equilibrating at $P = 0.01$ for $t = 6 \times 10^4$; and (iii) subsequently recompressing to $P = 1$ using the same $\dot{P}$ applied during decompression. An example time series of the resulting density is shown in Fig. 3(a). We observed that as pressure, and thus density, decrease, these stacks disintegrate, resulting in an A-B liquid at low density. Upon subsequent compression, beyond a certain pressure threshold, the condensation of the stiffer rings occurs, eventually reforming into a single stack. An animation of such a stable single stack is shown in the SM [59] (see movie 3) for the larger system of 1000 rings that we study.

We have conducted several such cycles, and the observations have consistently confirmed the stability of the stacks formed by the stiff rings, indicating that these structures are indeed stable. This process has been visualized in the animation provided in movie 4 in the SM [59]. To quantify the extent of stacking, we calculate the fraction of unstacked rings, f_{us}, adopting the criterion that a minimum of ten rings are needed to constitute a stack, i.e., $C_{\text{min}} = 10$. The time series for this data is depicted in Fig. 3(b), enabling us to plot f_{us} as a function of density. Given that decompression and compression occur at a finite rate, hysteresis is observed during the melting and freezing of the single stack; this phenomenon is illustrated in Figs. 3(c) and 3(d), with data for system sizes of 400 and 1000 rings demonstrating the robustness of our findings. By determining the fraction of unstacked rings and setting $f_{\text{us}} = 0.5$ as the threshold for identifying the presence of a stacked state among the B-type rings, we establish the bounds for the stability of the single stack. The data points obtained from our runs across various compositions are indicated in the phase diagram [see Fig. 2(b)]. Through this analysis, we conclude

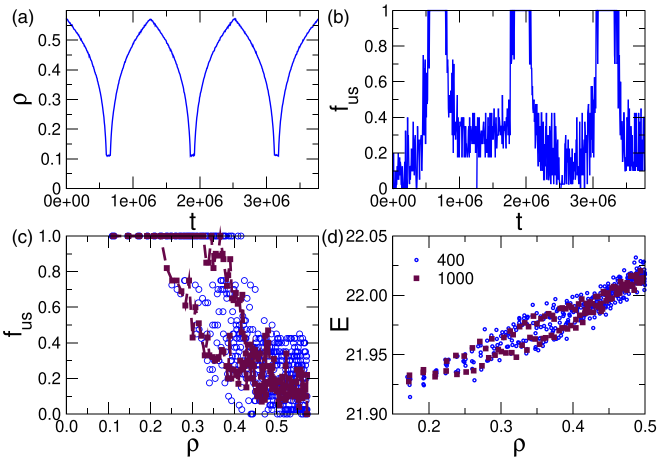

FIG. 3. During the pressure cycle, for the 90:10 mixture: time evolution of (a) density ρ, (b) fraction of unstacked rings, f_{us}, using a criteria that a stack has minimum size $C_{\text{min}} = 10$. Gathering data from such time series, hysteresis loops obtained for the variation of (c) fraction of unstacked rings, (d) potential energy (E), with density. In (a)–(d), data in blue corresponds to a system of 400 rings and data in maroon corresponds to 1000 rings.

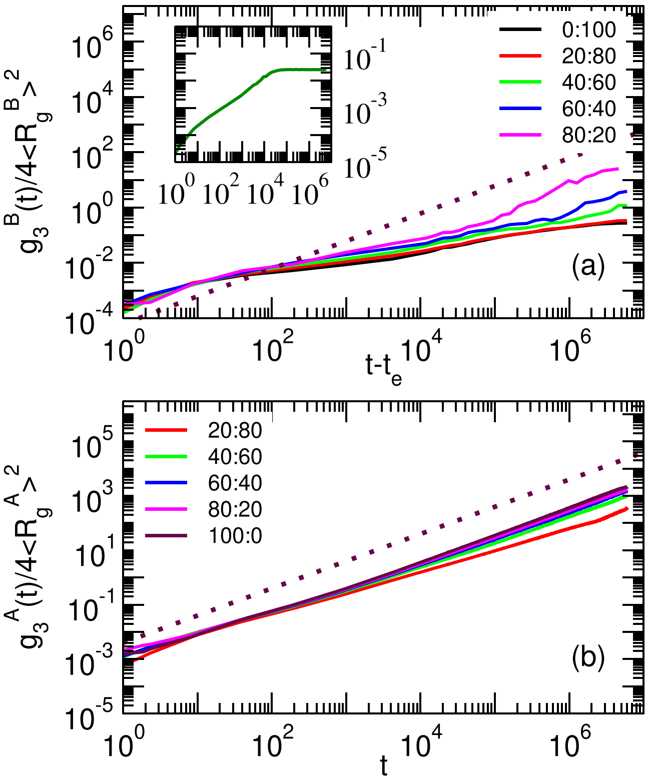

FIG. 4. Mean squared displacement of the center of mass of the single rings, $g_3(t)$, for (a) B-type rings, measured relative to $t_e = 6 \times 10^3$ (i.e., time since quench), and (b) A-type rings (time averaged), at different compositions as labeled. In both panels, the dotted line corresponds to linear behavior, i.e., $\sim t$, indicative of diffusive dynamics. The inset of (a) shows $g_3(t)$ measured relative to the center of mass of the single stack formed by the rings for the case of 90:10 composition.

that single stacks invariably form for ρ_A values exceeding these bounds at low ρ_B values.

E. Dynamical features

So far, we have focused on the structural aspects of our observations with the changing composition of binary mixtures. An important issue that needs addressing is whether the observed structures are in equilibrium. Specifically, we investigate the evolution of the dynamically arrested state of the pure 100:0 composition of the stiffer B-type rings with the progressive insertion of flexible A-type rings. These dynamical aspects are examined through the mean-square displacement (MSD), $g_3(t)$, of the center of mass of the rings. In Fig. 4, we present the MSD data for the two types of rings separately, in subpanels (a) and (b).

First, we focus on the dynamics of the B-type rings [see Fig. 4(a)]. In the pure 100:0 composition, they exhibit long-term dynamical arrest, as previously reported [42]. With the incremental addition of the more flexible A-type rings, the dynamics continue to display long-term localization, i.e., the existence of a plateau where the plateau height increases with dilution. This observation holds even for a 60:40 mixture, suggesting that the stiffer rings remain in a glassy state. As the concentration of B-type rings decreases, they form spatially inhomogeneous structures that are dynamically arrested, which could be characterized as gellike. Given the observed long-term glassiness, we average over four independent uncorrelated initial states and measure the dynamics of individual rings relative to a waiting time t_e (i.e., in terms of $t - t_e$) after the quench to the considered state point. The initial structures are generated via thermal quenches from $T = 5$ to $T = 1$, under isobaric conditions of $P = 1$, followed by a waiting period of $t_e = 6 \times 10^3$.

In the case of a 90:10 mixture, there is an observed tendency toward long-time diffusion for the stiff rings. However, when measuring the mean-square displacement (MSD) in the reference frame of the center of mass of the single stack, it becomes apparent that the rings remain stationary at long times, as shown in the inset of Fig. 4(a). This observation suggests that the long-time diffusion is attributable to the movement of the stack as a whole, while minimal structural rearrangements occur within the stack itself. Such a bound state likely arises from the peripheral intertwining of the rings within the stack, as is evidenced via the animation shown in movie 3 [59].

For the flexible A-type rings [see Fig. 4(b)], long-time diffusion is observed in all cases. Here, $g_3(t)$ is averaged over time origins within a trajectory after the stabilization of energy fluctuations. It is noteworthy that when the fraction of A-type rings is small (e.g., up to an A:B ratio of ~40:60), a pronounced transient subdiffusive regime is evident in their mean-square displacement, i.e., $g_3(t)$ grows sublinearly with time before reaching eventual long-time diffusion [see Fig. 4(b)]. Such transient behavior echoes the motion of interacting particles in an environment of quenched random soft obstacles [63–65]. A similar constrained motion is observed here in this composition regime: with the onset of stacking among the stiffer B-type rings, albeit randomly oriented (see Fig. 1), tubular channels form, creating a labyrinthine porous structure. This structure constitutes the only accessible space for the flexible rings to navigate [66]. As the fraction of B-type rings is further diluted, leading to stacked ordering, more free space becomes available for the A-type rings, thus leading to purely diffusive motion.

Via the analysis of the dynamical behavior of the rings, we deduce that the incorporation of flexible rings results in the initial coexistence of a glassy structure formed by the stiffer B-type rings with a liquid phase formed by the highly flexible A-type rings. Eventually, under isobaric conditions and at higher concentrations of the A-type rings, the coexisting structure transitions into a columnarly ordered, spatially inhomogeneous stacked structure of the stiffer B-type rings. Given the glassy dynamics of the stiffer rings, the structures they form at different densities are history-dependent, potentially leading to kinetically trapped states.

F. Varying stiffness ratio

The observed demixing of the two species of rings within the binary mixture bears resemblance to depletion-induced phase separations noted in other soft matter systems [67]. However, the ordered conformations of the stiffer ring polymers into stacks, as discovered in this study, represent a phenomenon arising from the asymmetry in the deformability of the constituent objects. To gain further insight into

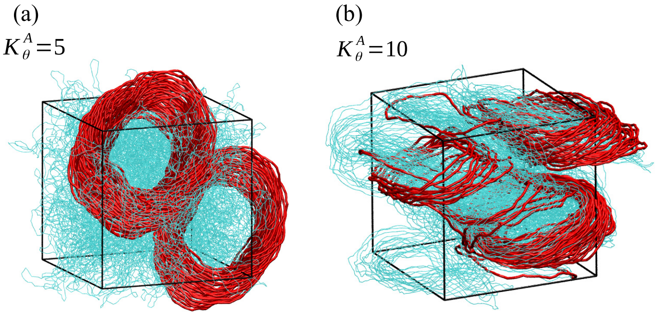

FIG. 5. Snapshots of the binary mixture with different K_θ^A values for A-type rings, viz. for (a) $K_\theta^A = 5.0$ and (b) $K_\theta^A = 10.0$ for the 80:20 mixture at pressure $P = 1.0$ and $K_\theta^B = 20.0$, with A-type rings shown in cyan and B-type rings shown in red.

the role of asymmetry, we simulated systems with varying stiffness ratios by altering the flexibility of the A-type rings (e.g., $K_\theta^A = 5.0$ and 10.0), while maintaining K_θ^B constant at 20.0. We examined the impact of this variation at a specific compositional state point, namely A:B = 80:20, where the stiffer B-type rings demonstrate a distinct stacked structure.

As shown in Fig. 5(a), altering K_θ^A from 1.0 to 5.0 does not significantly affect the structure of the B-type rings' stacks. However, at $K_\theta^A = 10.0$, the stack of B-type rings disintegrates, as shown in Fig. 5(b). This observation indicates that the depletion interactions between B-type rings diminish in the presence of stiffer A-type rings. Indeed, for $K_\theta^A = 10.0$, we note a competition for stacking and aggregation between the A-type and B-type rings (see movie 5 in the SM [59]). Previously, we have demonstrated that, at the operational pressure of $P = 1$, systems with $K_\theta^A = 10.0$ assume an elongated rod-type shape in the bulk phase [42]. In Fig. 5(b), we find that such rod-type rings are also capable of forming ordered stacks. This behavior is quantified by an observed increase in the stacking of the less stiff polymers ($K_\theta^A = 10.0$), as detailed in the Supplemental Material (see Sec. SII, Fig. S5, and movie 5). Consequently, the critical value for stiffness difference, at which a distinct coexisting ordered structure for the stiffer ring polymers becomes apparent, is identified to be between $5.0 \leqslant K_\theta^A \leqslant 10.0$ for $K_\theta^B = 20.0$ in this study.

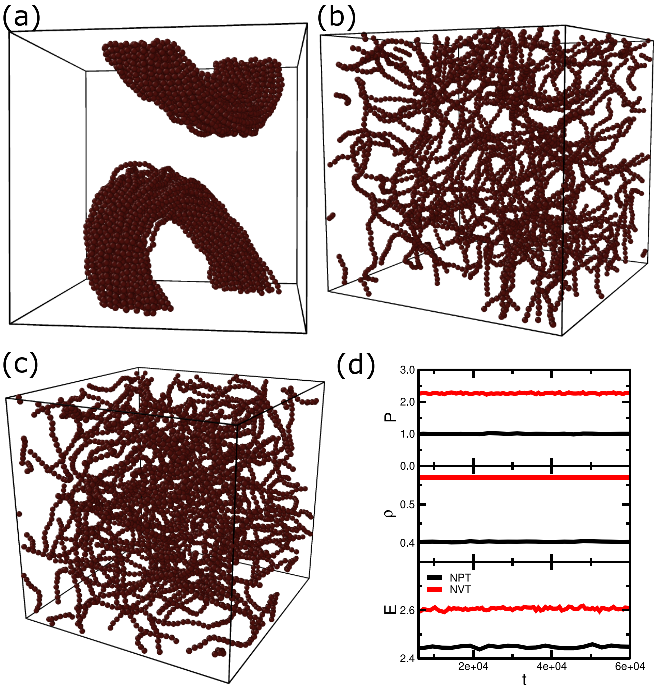

FIG. 6. (a) Initial stacked structure formed by 400 stiff ring polymers ($K_\theta = 20$) at ambient pressure of $P = 1$ and ambient temperature $T = 1$ for 90:10 composition, in coexistence with flexible ring polymers ($K_\theta = 1$). After the flexible rings are replaced by monomers, emergent equilibrium state of the stiff rings shown for (b) NPT condition $P = 1, T = 1$, (c) NVT condition $\rho = 0.57$, $T = 1$. (d) Equilibrium data for (i) pressure, (ii) density, (iii) potential energy of the mixture of stiff rings and colloids, under NPT, NVT conditions.

G. Mixture of stiff rings and colloidal particles

Finally, we have probed the significance of A-type flexible rings ($K_\theta = 1$) as a depleting agent in the stack formation by B-type stiffer rings ($K_\theta = 20$). This investigation was conducted by replacing the flexible rings with a collection of colloidal particles, which are comparable in size to the monomers constituting the polymers. These colloidal particles, in theory, can generate a depletion potential for the larger soft objects, specifically the stiffer B-type rings. Toward this, we started from the emergent stacked state formed by the 400 stiff rings at a 90:10 composition under ambient pressure of $P = 1$; see Fig. 6(a). In this setup, we replaced the flexible rings with monomers by severing the bonds that connect these polymers; thus, we maintained the same number of monomers as before, but now they are not linked to form flexible polymers. The interactions among the monomers, as well as between the monomers and the monomers constituting the stiff rings, were kept unchanged from the previous setup.

Thereafter, using this mixture of stiff rings and colloids as the initial configuration, we conducted molecular dynamics (MD) simulations under both NPT ($P = 1, T = 1$) and NVT ($\rho = 0.57, T = 1$) conditions over an extended time period. The data corresponding to pressure, density, and potential energy are presented in Fig. 6(d). The primary observation is that, under both ambient thermal states, the stack no longer remains intact; instead, it disintegrates and forms a liquid phase of stiff rings [see Figs. 6(b) and 6(c)]. Consequently, such an assembly of colloidal particles does not act as an effective depleting agent to facilitate stack formation at this state point. Notably, under NPT conditions, the overall density decreases to a mean value of 0.4, suggesting that the system becomes less compressible. This is further evidenced by an increase in pressure to around 2.2 under NVT conditions, as shown in Fig. 6(d).

This investigation underscores the crucial role that flexible $K_\theta = 1$ rings play in the demixing process, leading to the formation of stacks by the stiff rings. However, our study focused solely on colloidal particles of the same size (σ) as the monomers, whereas the flexible A ring has a radius of gyration $R_g \approx 4.2\sigma$ (see Fig. S3 in the Supplemental Material [59]). Therefore, further research is required to examine mixtures of stiff rings with colloidal particles of various sizes, under different thermal conditions, to assess the potential for stacking through demixing. Such studies would contribute to a deeper understanding of how the depletion mechanism is influenced by both the size and flexibility of the colloids.

IV. DISCUSSION AND CONCLUSIONS

In this study, we have employed extensive molecular dynamics simulations to explore the phase behavior of a binary mixture of ring polymers, differentiated by stiffness, at a fixed pressure. Beginning with a system-wide topological glass of stiff ring polymers at an ambient pressure of $P = 1.0$, our findings illustrate that the disordered state transitions along the isobaric path. The system reorganizes to form an ordered stack as the proportion of highly flexible ring polymers increases. This reorganization sees the diminishing and eventual disappearance of orthogonal threading, which is critical for the formation of the initial topological glass, upon the dilution of stiffer rings. At intermediate compositions, our dynamic analysis uncovers a disordered ensemble of smaller-sized stacks, oriented in various directions.

These insights enable us to propose a tentative phase diagram in the ρ_A, ρ_B space for this binary polymer mixture with contrasting stiffness. At low concentrations of both polymer types, a liquid phase comprising both flexible and stiff rings is observed. Increasing the concentration of flexible rings leads to the demixing and ordered stacking of the stiff rings. At higher ρ_B values, with an increase in ρ_A, the stiff rings demix to form a gel-like structure, coexisting with the liquid phase of flexible rings. At the highest ρ_B values, the topological glass formed by stiff rings also serves as a porous medium for the exploration by flexible rings. In all scenarios, a high ρ_A concentration results in a glassy phase of flexible rings coexisting with the structures formed by stiff rings. Future research will aim to validate this projected phase behavior.

A particularly intriguing observation is that, contrary to typical demixing scenarios where clear spatial segregation occurs between the demixed states, such as seen in mixtures of linear polymers of varying stiffness, the more flexible rings in our study inhabit the interior spaces of the columnar phase formed by the stiff rings. The energetics behind the stabilization of this columnar stack, alongside the interface with the liquid phase of flexible rings, warrants further investigation. Moreover, our experiments reveal that the ordered stacking into a singular cluster destabilizes as the stiffness asymmetry between the rings decreases. Instead, we observe formations of stack islands, hinting at potential micro-demixing phenomena that demand more detailed exploration.

ACKNOWLEDGMENTS

We thank the HPC facility at the Institute of Mathematical Sciences for computing time. P.C. and S.V. also acknowledge support via the subproject on the Modeling of Soft Materials within the IMSC Apex project, funded by Department of Atomic Energy. We also thank J. Horbach for the interesting discussions.

---

[1] A. Yethiraj and A. van Blaaderen, Nature (London) **421**, 513 (2003).
[2] C. I. Zoldesi and A. Imhof, Adv. Mater. **17**, 924 (2005).
[3] B. Li, D. Zhou, and Y. Han, Nat. Rev. Mater. **1**, 15011 (2016).
[4] A. van Blaaderen, Nature (London) **439**, 545 (2006).
[5] Z. Cheng, W. B. Russel, and P. Chaikin, Nature (London) **401**, 893 (1999).
[6] C. P. Royall, W. C. Poon, and E. R. Weeks, Soft Matter **9**, 17 (2013).
[7] P. K. Bommineni, M. Klement, and M. Engel, Phys. Rev. Lett. **124**, 218003 (2020).
[8] K. L. Young, M. L. Personick, M. Engel, P. F. Damasceno, S. N. Barnaby, R. Bleher, T. Li, S. C. Glotzer, B. Lee, and C. A. Mirkin, Angew. Chem., Int. Ed. **52**, 13980 (2013).
[9] H. N. W. Lekkerkerker and R. Tuinier, *Colloids and the Depletion Interaction*, Lecture Notes in Physics, Vol. 833 (Springer, Dordrecht, 2011).
[10] A. S. Karas, J. Glaser, and S. C. Glotzer, Soft Matter **12**, 5199 (2016).
[11] S. Park, H. Hwang, and S.-H. Kim, J. Am. Chem. Soc. **144**, 18397 (2022).
[12] K. Miyazaki, K. Schweizer, D. Thirumalai, R. Tuinier, and E. Zaccarelli, J. Chem. Phys. **156**, 080401 (2022).
[13] S. Asakura and F. Oosawa, J. Chem. Phys. **22**, 1255 (1954).
[14] M. Dijkstra, R. van Roij, and R. Evans, Phys. Rev. Lett. **81**, 2268 (1998).
[15] R. Dickman, P. Attard, and V. Simonian, J. Chem. Phys. **107**, 205 (1997).
[16] M. Dijkstra, R. Roij, and R. Evans, Phys. Rev. Lett. **82**, 117 (1999).
[17] H. Kobayashi, P. B. Rohrbach, R. Scheichl, N. B. Wilding, and R. L. Jack, Phys. Rev. E **104**, 044603 (2021).
[18] H. Wu, K. Song, W.-R. Chen, J. Song, L. Porcar, and Z. Wang, Phys. Rev. Res. **3**, 033271 (2021).
[19] E. Vermolen, A. Kuijk, L. Filion, M. Hermes, J. Thijssen, M. Dijkstra, and A. Van Blaaderen, Proc. Natl. Acad. Sci. USA **106**, 16063 (2009).
[20] S. Mukhopadhyay and J. Peixinho, Phys. Rev. E **84**, 011302 (2011).
[21] H. A. Makse, D. L. Johnson, and L. M. Schwartz, Phys. Rev. Lett. **84**, 4160 (2000).
[22] V. M. O. Batista and M. A. Miller, Phys. Rev. Lett. **105**, 088305 (2010).
[23] A. Boromand, A. Signoriello, F. Ye, C. S. O'Hern, and M. D. Shattuck, Phys. Rev. Lett. **121**, 248003 (2018).
[24] D. Michieletto and M. S. Turner, Proc. Natl. Acad. Sci. USA **113**, 5195 (2016).
[25] D. Michieletto, N. Nahali, and A. Rosa, Phys. Rev. Lett. **119**, 197801 (2017).
[26] D. Michieletto, D. Marenduzzo, E. Orlandini, and M. S. Turner, Polymers **9**, 349 (2017).
[27] M. A. Ubertini, J. Smrek, and A. Rosa, Macromolecules **55**, 10723 (2022).
[28] M. Q. Tu, O. Davydovich, B. Mei, P. K. Singh, G. S. Grest, K. S. Schweizer, T. C. O'Connor, and C. M. Schroeder, ACS Polymers Au **3**, 307 (2023).

[29] S. P. Obukhov, M. Rubinstein, and T. Duke, Phys. Rev. Lett. **73**, 1263 (1994).

[30] S. P. Obukhov, M. Rubinstein, and R. H. Colby, Macromolecules **27**, 3191 (1994).

[31] D. G. Tsalikis, V. G. Mavrantzas, and D. Vlassopoulos, ACS Macro Letters **5**, 755 (2016).

[32] Z. E. Dell and K. S. Schweizer, Soft Matter **14**, 9132 (2018).

[33] T. Sakaue, Soft Matter **14**, 7507 (2018).

[34] J. Smrek, I. Chubak, C. N. Likos, and K. Kremer, Nat. Commun. **11**, 26 (2020).

[35] I. Chubak, C. N. Likos, and J. Smrek, Mol. Phys. **119**, e1883140 (2021).

[36] I. Chubak, C. N. Likos, K. Kremer, and J. Smrek, Phys. Rev. Res. **2**, 043249 (2020).

[37] M. Z. Slimani, P. Bacova, M. Bernabei, A. Narros, C. N. Likos, and A. J. Moreno, ACS Macro Letters **3**, 611 (2014).

[38] M. Bernabei, P. Bacova, A. J. Moreno, A. Narros, and C. N. Likos, Soft Matter **9**, 1287 (2013).

[39] P. Poier, C. N. Likos, A. J. Moreno, and R. Blaak, Macromolecules **48**, 4983 (2015).

[40] P. Poier, P. Bačová, A. J. Moreno, C. N. Likos, and R. Blaak, Soft Matter **12**, 4805 (2016).

[41] M. Liebetreu and C. N. Likos, Appl. Polym. Mater. **2**, 3505 (2020).

[42] P. K. Roy, P. Chaudhuri, and S. Vemparala, Soft Matter **18**, 2959 (2022).

[43] A. Milchev, S. A. Egorov, J. Midya, K. Binder, and A. Nikoubashman, ACS Macro Letters **9**, 1779 (2020).

[44] S. A. Egorov, A. Milchev, A. Nikoubashman, and K. Binder, J. Phys. Chem. B **125**, 956 (2021).

[45] A. Milchev, S. A. Egorov, J. Midya, K. Binder, and A. Nikoubashman, Polymers **13**, 2270 (2021).

[46] R. Staňo, C. N. Likos, and J. Smrek, Soft Matter **19**, 17 (2022).

[47] M. C. Merola, D. Parisi, D. Truzzolillo, D. Vlassopoulos, V. D. Deepak, and M. Gauthier, J. Rheol. **62**, 63 (2018).

[48] D. Parisi, M. Camargo, K. Makri, M. Gauthier, C. N. Likos, and D. Vlassopoulos, J. Chem. Phys. **155**, 034901 (2021).

[49] D. Frenkel, Nat. Mater. **14**, 9 (2015).

[50] S. A. Egorov, Macromol. Theory Simul. **31**, 2100065 (2022).

[51] I. Chubak, C. N. Likos, and S. A. Egorov, J. Phys. Chem. B **125**, 4910 (2021).

[52] K. Kremer and G. S. Grest, J. Chem. Phys. **92**, 5057 (1990).

[53] J. D. Halverson, W. B. Lee, G. S. Grest, A. Y. Grosberg, and K. Kremer, J. Chem. Phys. **134**, 204904 (2011).

[54] J. D. Halverson, W. B. Lee, G. S. Grest, A. Y. Grosberg, and K. Kremer, J. Chem. Phys. **134**, 204905 (2011).

[55] J. D. Weeks, D. Chandler, and H. C. Andersen, J. Chem. Phys. **54**, 5237 (1971).

[56] M. Doi and S. Edwards, *The Theory of Polymer Dynamics* (Oxford University Press, Oxford, 1988).

[57] F. Guo, K. Li, J. Wu, L. He, and L. Zhang, Polymers **12**, 2659 (2020).

[58] A. P. Thompson, H. M. Aktulga, R. Berger, D. S. Bolintineanu, W. M. Brown, P. S. Crozier, P. J. in 't Veld, A. Kohlmeyer, S. G. Moore, T. D. Nguyen, R. Shan, M. J. Stevens, J. Tranchida, C. Trott, and S. J. Plimpton, Comput. Phys. Commun. **271**, 108171 (2022).

[59] See Supplemental Material at http://link.aps.org/supplemental/10.1103/PhysRevMaterials.8.045601 for simulation details and other analysis.

[60] S. Nosé, J. Chem. Phys. **81**, 511 (1984).

[61] G. J. Martyna, M. L. Klein, and M. Tuckerman, J. Chem. Phys. **97**, 2635 (1992).

[62] S. Nosé and M. Klein, Mol. Phys. **50**, 1055 (1983).

[63] S. K. Schnyder, M. Spanner, F. Höfling, T. Franosch, and J. Horbach, Soft Matter **11**, 701 (2015).

[64] S. K. Schnyder and J. Horbach, Phys. Rev. Lett. **120**, 078001 (2018).

[65] V. Vaibhav, J. Horbach, and P. Chaudhuri, J. Chem. Phys. **156**, 244501 (2022).

[66] The effective diameter of these tubes (d_{cav}) is proportional to the radius of gyration of the B-type rings (R_g^B), *i.e.*, $d_{\text{cav}} \sim 2 \times 14.5\sigma$, which allows for the directed motion of the flexible rings.

[67] R. Tuinier, J. Rieger, and C. G. De Kruif, Adv. Colloid Interface Sci. **103**, 1 (2003).